ACCOUNTS
of chemical research

The Electronic Properties of Superatom States of Hollow Molecules

MIN FENG,[†] JIN ZHAO,[†,§] TIAN HUANG,[†] XIAOYANG ZHU,[‡] AND HRVOJE PETEK*,[†]

[†]*Department of Physics and Astronomy and Petersen Institute of NanoScience and Engineering, University of Pittsburgh, Pittsburgh, Pennsylvania 15260, United States,* [‡]*Department of Chemistry and Biochemistry, University of Texas, Austin, Texas 78712, United States, and* [§]*Hefei National Laboratory for Physical Sciences at Microscale, University of Science and Technology of China, Hefei, Anhui, China*

RECEIVED ON OCTOBER 27, 2010

CONSPECTUS

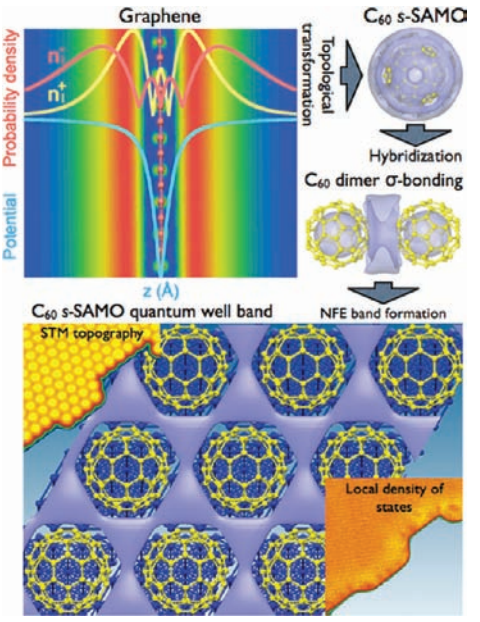

Electronic and optical properties of molecules and molecular solids are traditionally considered from the perspective of the frontier orbitals and their intermolecular interactions. How molecules condense into crystalline solids, however, is mainly attributed to the long-range polarization interaction. In this Account, we show that long-range polarization also introduces a distinctive set of diffuse molecular electronic states, which in quantum structures or solids can combine into nearly-free-electron (NFE) bands. These NFE properties, which are usually associated with good metals, are vividly evident in sp^2 hybridized carbon materials, specifically graphene and its derivatives.

The polarization interaction is primarily manifested in the screening of an external charge at a solid/vacuum interface. It is responsible for the universal image potential and the associated unoccupied image potential (IP) states, which are observed even at the He liquid/vacuum interface. The molecular electronic properties that we describe are derived from the IP states of graphene, which float above and below the molecular plane and undergo free motion parallel to it. Rolling or wrapping a graphene sheet into a nanotube or a fullerene transforms the IP states into diffuse atom-like orbitals that are bound primarily to hollow molecular cores, rather than the component atoms. Therefore, we named them the superatom molecular orbitals (SAMOs). Like the excitonic states of semiconductor nanostructures or the plasmonic resonances of metallic nanoparticles, SAMOs of fullerene molecules, separated by their van der Waals distance, can combine to form diatomic molecule-like orbitals of C_{60} dimers. For larger aggregates, they form NFE bands of superatomic quantum structures and solids.

The overlap of the diffuse SAMO wavefunctions in van der Waals solids provides a different paradigm for band formation than the valence or conduction bands formed by interaction of the more tightly bound, directional highest occupied molecular orbitals (HOMOs) or the lowest unoccupied molecular orbitals (LUMOs). Therefore, SAMO wavefunctions provide insights into the design of molecular materials with potentially superior properties for electronics.

Physicists and chemists have thought of fullerenes as atom-like building blocks of electronic materials, and superatom properties have been attributed to other elemental gas-phase clusters based on their size-dependent electronic structure and reactivity. Only in the case of fullerenes, however, do the superatom properties survive as delocalized electronic bands even in the condensed phase. We emphasize, however, that the superatom states and their bands are usually unoccupied and therefore do not contribute to intermolecular bonding. Instead, their significance lies in the electronic properties they confer when electrons are introduced, such as when they are excited optically or probed by the atomically sharp tip of a scanning tunneling microscope.

We describe the IP states of graphene as the primary manifestation of the universal polarization response of a molecular sheet and how these states in turn define the NFE properties of materials derived from graphene, such as graphite, fullerenes, and nanotubes. Through low-temperature scanning tunneling microscopy (LT-STM), time-resolved two-photon photoemission spectroscopy (TR-2PP), and density functional theory (DFT), we describe the real and reciprocal space electronic properties of SAMOs for single C_{60} molecules and their self-assembled 1D and 2D quantum structures on single-crystal metal surfaces.

Published on the Web 03/17/2011 www.pubs.acs.org/accounts
10.1021/ar1001445

Introduction

Cohesive energy of molecular materials has contributions from short-range chemical bonding and long-range polarization interactions.[1] The short-range interactions give molecules their chemical identity, whereas the long-range interactions define how molecules interact with each other in supramolecular structures such as molecular crystals, proteins, cell membranes, etc. These interactions also define how electronic charge is transported within and among molecules in molecular materials.

The long-range polarization interaction between atoms, molecules, and surfaces is universal because it arises through correlations between fluctuating charge distributions and fields. In this Account, we examine the fundamental polarization interaction between an external charge and a molecular sheet, which gives rise to the long-range image potential with the associated IP states, and its manifestations in the superatom electronic properties of hollow molecules, their nanostructures, and solids derived from molecular sheets.

To understand how polarization leads to new electronic states, we begin with the electronic structure of graphene. The electronic potential of graphene can be constructed from contributions from the Coulomb, the short-range exchange−correlation, and the long-range polarization interactions. Solutions of the Schrödinger equation for the combined potential describe the electronic structure over a range of length and energy scales that are relevant to chemical bonding, optical response, and electron transport of graphene and its derivatives. The solutions obtained in a density functional theory (DFT) calculation can be classified according to their principal quantum number, which specifies the number of nodes parallel to the molecular plane (the carbon sheet); the $n = 1$ and 2 solutions correspond to the familiar σ- and π-orbitals, respectively, with zero and one nodal planes. Four valence electrons per carbon atom distributed between the 2s and 2p orbitals occupy three filled σ-bands and two degenerate half-filled π-bands. At the Γ-point of the 2D Brillouin zone, energy gaps of 34 and 20 eV, respectively, separate the σ- and π-bonding from the corresponding antibonding bands;[2,3] at the K- and K'-points, however, the conical π-bands intersect at point-like Fermi surfaces (Figure 1).[4] The quasiparticles of graphene occupying these so-called Dirac cones impart exotic electronic and optical properties that are of significant topical interest.[5]

Whereas the well-known σ- and π-bands have density maxima at the atomic cores and along the chemical bonds,

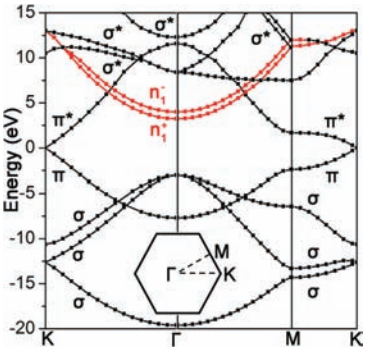

FIGURE 1. The calculated band structure of graphene. Only the first members of the even (n_1^+) and odd (n_1^-) IP states series are shown by red lines.

we are primarily interested in the less-explored $n = 3$ solution for graphene. The many-body screening of the Coulomb field of an external charge creates an oppositely charged image in a polarizable medium.[6] The induced Coulomb potential dominates the long-range interaction between an external charge and a polarizable surface. This potential supports $n \geq 3$ states of graphene, which converge asymptotically to the vacuum level, E_v, in a dual Rydberg series of even and odd parity.[2] Without inclusion of the polarization, DFT calculations cannot give accurate energies and spatial distributions of these IP states.

We first describe the IP states of graphene because they are the physical origin of the superatom states. Next, we explore by experiment and theory how IP states evolve by interlayer interaction into the interlayer states of graphite, and through topological transformations (wrapping and rolling) into atom-like orbitals of graphitic hollow molecules. We show that these atom-like states, in turn, form nearly-free-electron (NFE) bands of fullerene and nanotube quantum structures or solids. Finally, we speculate on the potential of exploiting $n = 3$ states of hollow molecules in molecular electronics.

Image Potential States of Graphene

We begin by providing a theoretical description of the $n \geq 3$ states, that is, the IP states, of molecular sheets. Although the $n = 3$ state of graphene is unoccupied, it nevertheless can impart striking chemical and physical properties to graphitic materials. For instance, the interlayer state, which is derived from the IP state of graphene, confers superconducting properties to intercalated graphite compounds and dominates the interstitial potential involved in charge transport in Li-ion batteries.[7,8] Whereas DFT and tight binding methods describe adequately the σ- and π-bands of graphene, they

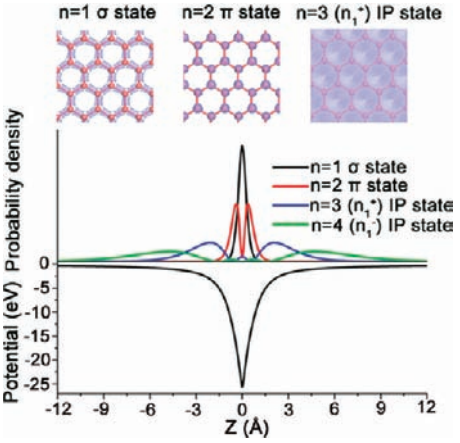

FIGURE 2. The effective surface-normal potential and the corresponding calculated probability densities of $n = 1-4$ states of graphene. Top panels show the top views of the $n = 1-3$ state probability densities at the Γ-point.

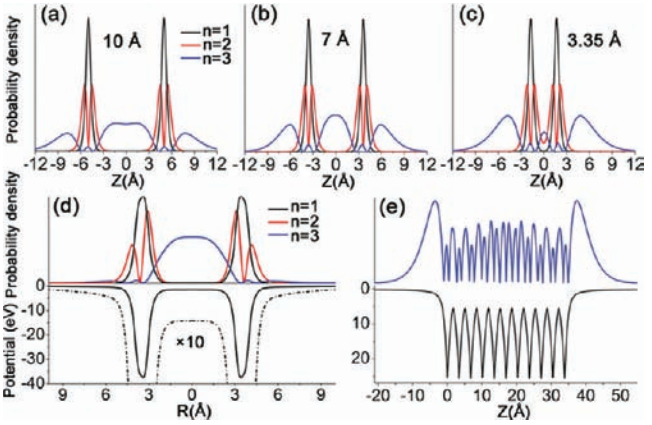

FIGURE 3. (a-c) The calculated probability densities of the $n = 1-3$ states of bilayer graphene for interlayer separations, respectively, of $d =$ 10.0, 7.0, and 3.35 Å. (d) The effective potential and calculated radial distributions of the $n = 1-3$ states of C_{60} molecule. (e) The calculated effective potential and IS band formed by interaction of the n_1^+ IP states of graphene for a 10-layer slab.

fail for the $n = 3$ and higher states, which are defined by both the short-range exchange−correlation (V_{xc}) and the long-range (V_{IP}) polarization potentials.[2] Therefore, to describe the electronic properties derived from IP states, we construct an empirical potential following the prescription for semi-infinite metal surfaces:[2,9] we splice the V_{xc} from DFT to the Coulomb potential (V_{IP}) at a distance $\pm z_i$ above and below the molecular sheet. Requiring that the obtained potential for a stack of graphene layers reproduce the known IP state energies of graphite defines z_i.[10,11] Thus calculated potential and probability densities for $n = 1-4$ states averaged in the graphene plane and top view are shown in Figure 2. The σ- and π-band charge densities are characteristic of aromatic molecules.[1] The more diffuse $n = 3$ and $n = 4$ solutions are the first even (n_1^+) and odd n_1^- IP states.[2] Like their semi-infinite counterparts on metals, the bilateral IP states of molecular sheets are characterized by pronounced n-dependent non-nuclear density maxima (Figure 2).[2] The IP states of epitaxial graphene on SiC substrate, where the even−odd symmetry is broken, have recently been observed by STM.[12]

Interlayer State of Graphite

When graphene sheets are stacked to form graphite, the NFE-IP states form a band, as was first described theoretically by Posternak et al.[13] Figure 3a−c shows how the so-called interlayer state (IS) is formed through overlap of IP states when two graphene sheets are brought together. The IS probability density is calculated by solving the Schrödinger equation for the sum of graphene potentials in Figure 2 to represent several graphene bilayers with different interstitial separations, d. The IS density between the basal planes depends strongly on d as it is reduced from 10 to 3.35 Å (Figure 3a−c). Because the interlayer distance of graphite, $d = 3.35$ Å, is comparable to the distance of the n_1^+ IP state density maximum from the graphene plane, where V_{xc} still dominates over V_{IP}, the IS is well described by DFT.[2,3,13,14] The competing effects of wave function overlap and confinement produce the maximum interlayer density of IS for $d \approx 7$ Å (Figure 3b). Confinement within smaller interlayer distances expells the probability density to the vacuum giving IS predominantly an IP character (Figure 3c). For the $n = 3$ band of a 10-layer graphite slab in Figure 3e, the dual IP−IS character of the NFE band is evident. In graphite, the strong interlayer interaction of $n \geq 3$ states causes the IS to disperse normal to the basal planes from 4.0 eV at the Γ-point (all energies are given relative to the Fermi level, E_F), where it has the maximum IP character, to 7.5 eV at the A-point, where it has the maximum IS character.[3] Because IP states are a universal consequence of the polarization interaction, we can conclude that the strongly 3D dispersive IS states are a universal property of layered quasi-2D solids.

The IS has been described by theory and characterized by inverse photoemission spectroscopy (IPS) for the intrinsic and Li intercalated graphite.[3,10,13] Although IP states and NFE bands derived from them exist several electronvolts above E_F, through doping with metal atoms, IS can be stabilized to below E_F,[7] thereby imparting novel electronic properties. IPS measurements show that intercalation stabilizes IS by ∼3 eV through interaction with 2s states of Li atoms. Stabilization of IS below E_F has been implicated in superconductivity of intercalated graphitic compounds such

as C_6Ca and related layered materials.[7] Moreover, in materials with two inequivalent atoms like hexagonal BN, opening up of a band gap in the π-bands can place IS at the conduction band minimum.[15,16]

Superatom States of Hollow Molecules

Having described the IP state of graphene, we next examine how topological transformations (wrapping or rolling) of graphene into fullerenes and nanotubes leads to superatom states. The bilateral n_1^+ and n_1^- IP states can be interpreted as the symmetric and antisymmetric linear combinations of degenerate semi-infinite wave functions on each side of the graphene plane. Curvature-induced symmetry breaking[17] lowers/raises the energy of IP states on the concave/convex side of the sheet. DFT calculations predict that the internal $n = 3$, $l = 0$ (linear momentum $k_{\|}$ transforms into orbital angular momentum l) NFE states of nanotubes or fullerenes are stabilized relative to the parent IP state.[16,18]

The electronic counterparts of IP states of graphene have been observed experimentally with femtosecond temporal and atomic spatial resolution, respectively, in spectroscopic time-resolved two-photon photoemission spectroscopy (TR-2PP) and low-temperature scanning tunneling microscopy (LT-STM) measurements for C_{60} molecules on noble metals.[18,19] Although the LUMO states of chemisorbed C_{60} have been studied extensively,[20−22] here we focus on the less explored 3−5 eV energy range where we discovered the $n = 3$ states.

The TR-2PP and LT-STM are complementary probes of the unoccupied electronic structure of metal/molecule interfaces. Each method can be used to introduce an additional electron, either from the metal substrate or the STM tip, into normally unoccupied resonances of chemisorbed molecules. In TR-2PP, a pair of ultrafast ($\leq$100 fs) optical pulses excites electrons from occupied initial to final states above E_v via unoccupied intermediate states. Photoelectron spectra recorded as a function of electron momentum and pump−probe delay reveal the intermediate electronic states and their relaxation dynamics.[23] The intermolecular electronic interactions among molecular orbitals lead to formation of electronic bands. These interactions can be quantified through measurements of energy-parallel momentum dispersion relation, which give the electronic bandwidth and the effective band-mass m_{eff}.[1,23−26]

STM measurements provide complementary real-space information on the interfacial electronic structure and interactions. In addition to topography, differential current−voltage measurements (dI/dV) with STM provide spatially resolved spectra and maps of the local density of states (LDOS). For bias voltages up to ~3 V, the HOMO, and LUMO − LUMO + 2 states of C_{60} molecules on metal and semiconductor surfaces have been characterized through their dI/dV spectra and LDOS.[20−22] At higher voltages, $z-V$ modulation at constant current offers an alternative spectroscopic method. Tunneling resonances produce plateaus in $z-V$ scans.[27] The numerically differentiated dz/dV spectra, such as those of a single C_{60} molecule in Figure 4, reveal peaks corresponding to the LUMO + 1, LUMO + 2, and superatom molecular orbital (SAMO) resonances.

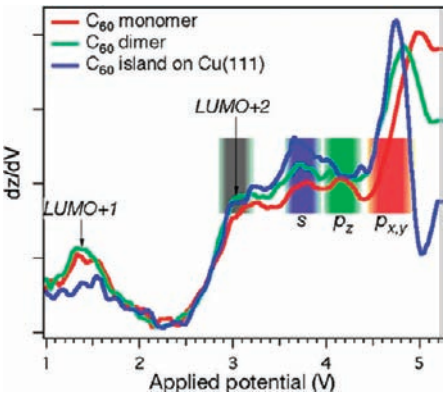

FIGURE 4. The dz/dV spectra identifying specific tunneling resonances of an isolated C_{60} molecule and dimer on Cu(110)-(2 × 1)-O surface and a quantum well on Cu(111) surface.[18]

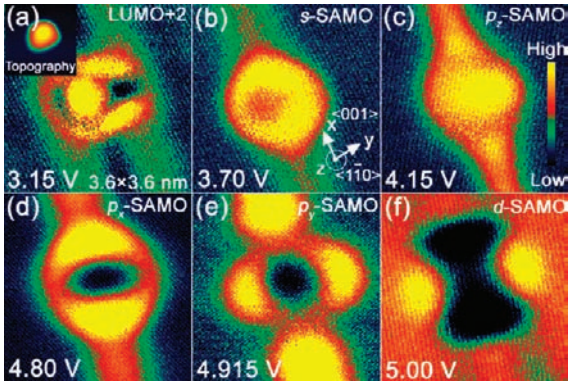

FIGURE 5. (a−f) The dI/dV images of LUMO + 2 and s-, p-, and d-SAMOs for a C_{60} molecule (topography is shown in the inset) on Cu(110)-(2 × 1)-O surface.[18]

Figure 5 shows the LDOS images of a single C_{60} molecule trapped in a one atom wide bare Cu trough on a Cu(110)-(2 × 1)-O reconstructed surface.[18] The dI/dV images are recorded for resonances revealed in Figure 4. At 3.15 V (Figure 5a), the LDOS shows the characteristic contrast within the C_{60} molecule corresponding to the π^*-orbitals of the LUMO + 2 state on the topmost carbon pentagon and hexagon.[18]

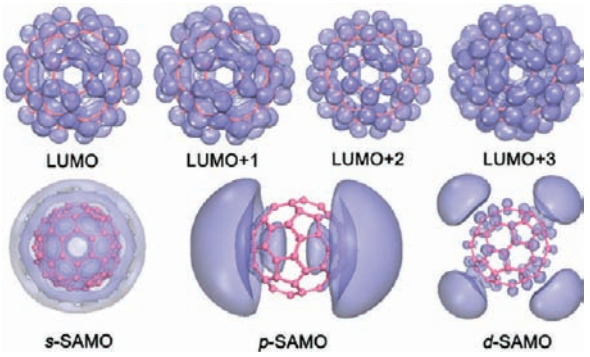

FIGURE 6. The calculated spatial distributions of LUMO−LUMO + 3, and s-, p-, and d-SAMOs of isolated C_{60} molecule.

To contrast the unoccupied electronic structure in different energy regions, Figure 5 juxtaposes the LDOS of LUMO + 2 with other images taken with higher bias voltages. Above 3.5 V, the intramolecular contrast in LDOS images vanishes. For example, at 3.70 V, the LDOS is nearly uniform over the entire molecule except for a characteristic dark spot above the topmost C_{60} hexagon. At 4.15 eV, the LDOS has the same symmetry but is more confined above the C_{60} molecule. At 4.80 and 4.915 V, respectively, the LDOS images have nodes bisecting the molecule in the (001) and $(1\bar{1}0)$ planes. Finally, the 5.00 V image has a quadrupolar LDOS distribution corresponding to nodes in both planes. By contrast to LUMO + 2, the LDOS of these diffuse orbitals is uncorrelated with atoms or bonds of the fullerene cage.

To explain the origin of these diffuse orbitals, we performed plane-wave DFT electronic structure calculations for the neutral, isolated C_{60}.[18] The calculated unoccupied orbitals reproduced in Figure 6 can be classified as either compact or diffuse. By projecting out the states with predominantly C-2p orbital character, we sift the diffuse states from the π^*-states. Thus identified diffuse orbitals are centered on the hollow core and evoke shapes of atomic s, p, and d orbitals corresponding, respectively, to $l = 0$, 1, and 2. Accordingly, we named them the superatom molecular orbitals (SAMOs), and labeled them according to their l and its surface projection m. Based on the energy and nodal structures, we attribute the images in Figure 5b−f to the s-, p_z-, p_y-, p_x-, and d-SAMOs.

Because the description of SAMOs requires a complete basis set, for example, plane-waves, they have largely escaped scrutiny by theory. A study by Martins et al. on the photoemission and IPS of C_{60} solid employed the plane-wave basis set and classified the states obtained for a self-consistent central potential of a hollow spherical shell according to their n and l.[28] The $n = 3$ solutions have also been found in calculations where C_{60} was described by a stabilized jellium shell.[29] Recently, Pavlyukh et al. described the electronic structure of spherical molecules in terms of the averaged angular momentum l, where SAMOs are a consequence of a radial potential and spherical symmetry.[30] The theoretical description of SAMOs and their LDOS imaging confirms them as the modes of a hollow spherical shell.

Accordingly, we solve the Schrödinger equation for the self-consistent radial potential obtained by angular averaging of the DFT potential. This potential and its solutions up to $n = 3$ are shown in Figure 3d. Similar to the bilayer graphene, the potential has a deep minimum on the carbon shell and a shallow attractive inner potential. For the shell diameter of 7.2 Å, V_{xc} mainly defines the inner potential; the long-range V_{IP} potential contributes significantly only outside the shell. The cross-sectional probability densities of C_{60} molecule (Figure 3d) and graphene monolayer and bilayer (Figures 2 and 3a−c) are similar for their tightly bound $n = 1$ and 2 states; the small asymmetry between the internal and external σ- and π-orbital densities of fullerenes has been attributed to the curvature-induced $\sigma-\pi$ mixing.[31]

By contrast to the σ- and π-orbitals, the intersheet interaction strongly affects the $n = 3$ states. Recall that for graphene bilayer, the $n = 3$ probability densities attain their interlayer maximum for $d \approx 7$ Å, which is comparable to C_{60} molecule diameter (Figure 3). Therefore, C_{60} is close to the ideal size for confining the maximum s-SAMO density within the carbon shell.[32] The accumulation of probability density within the C_{60} molecule can be attributed to both the shell curvature and its diameter.[16,32] As for atomic wave functions, the $l \geq 1$ wave functions have nodes intersecting the core, and therefore their densities within the carbon shell are reduced substantially with respect to s-SAMO.[32]

The unique property of s-SAMO that distinguishes it from a Rydberg state is the accretion of probability density within the molecular core. The higher energy $n = 4$ state being derived from the n_1^- state of graphene is mostly external to the carbon shell, and therefore, can be considered as the first member of a Rydberg series. Note that SAMO-like states with additional excitonic stabilization also appear as excitations in neutral C_{60} molecules.[33]

Finally, we consider the role of the Cu(110)-(2 × 1)-O surface. The LDOS of SAMOs of chemisorbed C_{60} molecules corresponds quite well to their theoretical description for isolated molecules. The anisotropic substrate primarily lifts degeneracy of the spatial components of p-SAMO but otherwise is a minor perturbation. We also calculated the electronic structure of C_{60} on Cu(110)-(2 × 1)-O surface and found that the LDOS at the

molecule−vacuum interface that is probed by STM is hardly perturbed by the interactions at the molecule−metal interface.

Formation of SAMO-Derived NFE Bands

Next we discuss how the interaction of SAMOs leads to formation of NFE bands of 1D and 2D quantum structures. The primary features of intermolecular interaction of SAMOs can be found in d*I*/d*V* images of fullerenes.[18,34,35] On Cu(110)-(2 × 1)-O surface along the ⟨001⟩ direction, occasional 0.76 nm wide bare Cu domains act as templates for self-assembly of single-molecule wide, up to fifty C_{60} molecules long (>50 nm), chains. The 0.36 nm unit cell of Cu(110) substrate defines the intermolecular spacing of 1.07 ± 0.02 nm, that is, ∼7% larger than the C_{60} molecule van der Waals diameter.[18] C_{60} molecules can assume two orientations corresponding to the opposite alignment of the topmost pentagon and hexagon in the ⟨1$\bar{1}$0⟩ direction[35] (see the images in Figure 7a).[18]

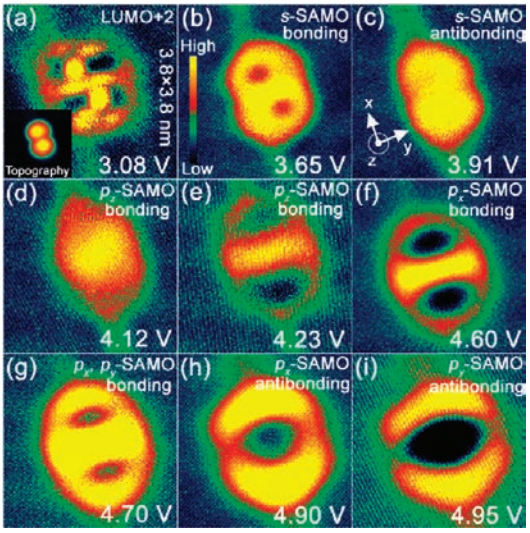

FIGURE 7. The d*I*/d*V* images of a C_{60} dimer on Cu(110)-(2 × 1)-O surface contrasting the LUMO + 2 (a) with the diatomic molecule-like orbitals of interacting SAMOs (b−i).

It is evident in Figure 7 that intermolecular interaction of SAMOs transforms the LDOS of the interacting orbitals. In the dimer image of LUMO + 2 (Figure 7a), π^*-orbitals largely retain the LDOS of a monomer (Figure 5a). By contrast, the energy-dependent changes in the LDOS of SAMOs can be understood by analogy to a diatomic molecule where the interacting atomic s and p orbitals form the bonding and antibonding molecular orbitals.[1] With increasing energy, the d*I*/d*V* images exhibit features of σ- and σ^*-bonding of s-SAMOs, π-bonding of p_z-SAMOs, σ- and σ^*-bonding of p_x-SAMOs, and π- and π^*-bonding of p_y-SAMOs.[18] We found similar intermolecular interactions of SAMOs of $Sc_3N@C_{80}$, an endohedral fullerene.[34]

Next we examine the SAMO-derived electronic properties in quantum structures. Figure 8 shows a topographic and several d*I*/d*V* images of a self-assembled chain of nine C_{60} molecules on a Cu(110)-(2 × 1)-O surface. The loss of molecular contrast in the LDOS of the chain portends that SAMOs form delocalized 1D bands. In discussing such images, we note that the applied bias voltage determines whether STM tunneling occurs into the Brillouin zone center or the boundary states. Moreover, electron bands with $m_{eff} > 0$ (band minimum at the Γ point), that is, s-σ, p_y-π, and p_z-π, are imaged differently from the hole bands with $m_{eff} < 0$ (minimum at the zone boundary), that is, p_x-σ^*. Indeed, LDOS corresponding to these bands can be identified in Figure 8 by comparison with the calculated SAMO orbital distributions for a C_{60} molecule chain in ref 32. Fitting the calculated energy−momentum dispersions gives m_{eff} of $1.0m_e$ for the s-σ and p-π bands and $-0.2m_e$ for the p_x-σ^* band (m_e is the free-electron mass), confirming that SAMOs combine into NFE bands.[1] A tight binding parametrization gives the respective hopping integrals β of 90 and −270 meV, corresponding to bandwidths of 360 and 1000 meV.[32]

We have also investigated the electronic structures of 2D quantum wells for one to several C_{60} molecule thick films. Figure 9 shows the topographic and LDOS images of a C_{60}

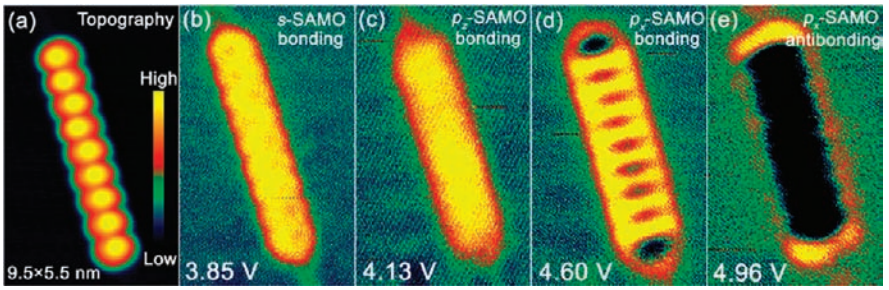

FIGURE 8. (a−e) The topography and d*I*/d*V* images of a linear chain of C_{60} molecules on the Cu(110)-(2 × 1)-O surface showing the 1D σ- and π-bands formed by interaction of SAMOs.

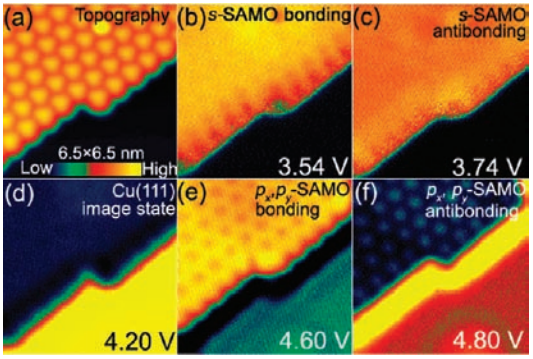

FIGURE 9. (a−f) The topography and d*I*/d*V* images of a C_{60} island on Cu(111) showing the 2D *s*- and p_x, p_y-SAMO ($m = 0$ and $m = \pm 1$) bands.

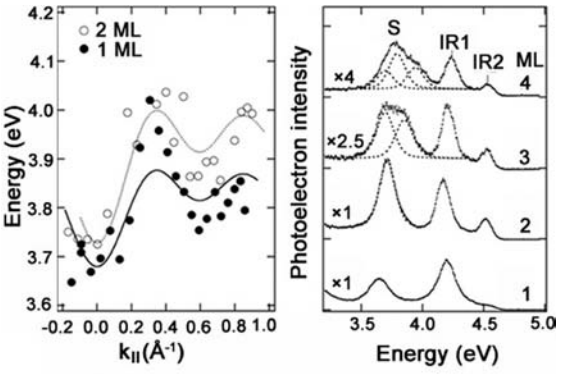

FIGURE 10. Right, 2PP spectra taken with 4.593 eV photons for C_{60} covered Au(111) surfaces at molecular film thicknesses of 1−4 monolayers (ML). IR1 and IR2 are assigned to IP resonances above the C_{60} overlayer, and S is assigned to the s-SAMO band. The dashed curves show deconvolution of multilayer film features into peaks that are split by the interlayer interaction. Left, Parallel dispersions of the s-SAMO band for 1 and 2 ML thick films. The curves are fits to a tight binding model.[19]

island on Cu(111). C_{60} molecules form a hexagonal 4 × 4 structure with 1.02 nm intermolecule distance defined by the 0.255 nm surface unit cell. Again, the LDOS images show SAMO delocalization into NFE bands. The LDOS at 3.74 V shows the complete loss of molecular contrast consistent with the 2D NFE band formation of s-SAMO.[32] The 4.2 V image shows the spatially complementary contrast arising from tunneling into the IP state of the bare Cu(111). These images (i) confirm that the diffuse contrast can be attributed to formation on the NFE band; (ii) illustrate that even though IP states disperse above E_v,[36] the STM probes mainly the DOS at the Γ-point; and (iii) delineate the electronic edge of the C_{60} island.

Next we examine two distinct features of the 4.6 V band in Figure 9. First, centered on each C_{60} molecule is a dark spot indicative of a wave function node. Second, the edge of the C_{60} island shows one-molecule wide dark contrast, which reverses to bright contrast at 4.8 V. The node piercing each molecule reflects the $m = \pm 1$ symmetry of the p_x- and p_y-SAMOs. For single molecules on an anisotropic surface (Figure 5), nodal planes identified the p_x- and p_y-SAMOs. For the isotropic Cu(111) surface, $m = \pm 1$ SAMOs are degenerate, so the orthogonal nodal planes collapse into a line at their intersection. The corrugation with the periodicity of the C_{60} lattice identifies the 4.6 V image with the zone boundary region of the $m = \pm 1$ band. Therefore, on the basis of these features, we attribute the 4.6 V LDOS to the p_x, p_y-SAMOs band.[18]

Concerning the C_{60} island edge, the inversion from the dark to bright contrast between 4.6 and 4.8 V is a consequence of dispersion of the $m = \pm 1$ SAMO band. Being a hole band, the bonding and antibonding characteristics, respectively, appear at the zone boundary (band minimum) and the Γ-point (band maximum).[1] The bright contrast of the island boundary is an edge state, that is, a 1D analog of a 2D surface state. Just as surface states appear by termination of a solid, so do edge and point states, respectively, appear at boundaries of 2D quantum wells and 1D quantum wires.[37,38] A finite system minimizes its free energy by accumulating the bonding charge density in its interior and by expelling the antibonding density to its boundary. These concepts also explain the line end (point state) dark and bright contrast of the p_x-SAMO in Figure 8e.

Next we consider the correspondence between the LT-STM and two-photon photoemission (2PP) studies of C_{60} overlayers on noble metals. Using angle- and time-resolved 2PP, Zhu, Harris, and co-workers have studied the unoccupied electronic structure of monolayer to multilayer thick C_{60} films on Cu(111), Ag(111), and Au(111) surfaces.[19,25,39−41]

Whether an electron is supplied externally by tunneling from an STM tip or internally by photoexcitation from the substrate, LT-STM and 2PP measure the same unoccupied states assuming that the electron−hole interaction is screened. Other differences may arise through a shift of electronic resonances by the Stark effect induced by the applied field of STM tip. The Stark shift of IP states is much larger than that for molecular states.[27] Moreover, differences in the wave function overlap and transition moments for the internal vs external electron transfer can influence the sensitivity of each technique.

The main point of comparison between LT-STM and 2PP is the 3.7 eV peak, which appears both in 2PP spectra of C_{60}/Au(111) surface (Figure 10) and d*z*/d*V* spectra of C_{60} on copper surfaces (Figure 4). In 2PP spectra, Zhu et al. found this state to disperse with both parallel and perpendicular

momenta. The right panel in Figure 10 shows a set of 2PP spectra of 1−4 monolayer (ML) films, which reveal three distinct unoccupied bands: the first two are IP resonances, "IR1" and "IR2". Below them is the peak labeled "S", which reveals its NFE characteristics through both its parallel dispersion and splitting with increasing film thickness above 2 ML. The splitting in thicker films is evidence for interaction that evolves into the 3D NFE band of C_{60} molecular crystal. The first monolayer is unique because C_{60} molecules are strongly polarized by the metal substrate. A tight binding model describes both the parallel dispersions and interlayer splittings with a $\beta = -33 \pm 3$ meV[19] corresponding to a bandwidth of $-12\beta = 400$ meV. The NFE character of the "S" state stands in strong contrast with the effectively nondispersive LUMO states that have also been studied by angle-resolved 2PP measurements for C_{60} on the Ag(111) surface.[25,32] Thus, the complementary 2PP and LT-STM measurements establish that, by contrast with the frontier orbitals of aromatic molecules,[42] the superatom states of hollow molecules can impart metal-like NFE properties to molecular solids, which could be of practical interest in molecular electronics.

Perspectives

In this Account, we have described the diffuse electronic states of molecular sheets and hollow molecules derived from them. We have shown by experiment and theory that above the familiar σ- and π - states that are defined by the constituent atomic core potentials, there exist $n = 3$ and higher states that belong to the image potential states and are defined by short-range exchange−correlation and long-range polarization potentials.[43] Although one needs to explore several electronvolts above E_F to discover the superatom electronic properties of C_{60} at energies where electronic relaxation would obviate charge transport, we envisage materials design strategies to enable exploitation of NFE properties of molecular sheets. For instance, whereas the IP states of graphene are unoccupied, by doping of graphite with intercalated metal atoms the IS can be stabilized to below E_F.[7] Our calculations predict the same outcome for the endohedral doping of C_{60} molecules and nanotubes with, for instance, noble metal atoms.[16,32] In other materials, the IP states can form the conduction band minima, either by opening a gap in the π-bands, as in hexagonal BN,[15] or by saturating the p-orbitals, as in graphane.[44]

As a general feature of hollow molecules, the exchange−correlation potential gives rise to NFE states with probability densities that can be mostly contained within their inner space,[16] which makes them of significant interest in optical and electronic applications, because they provide a different paradigm for the intra- and intermolecular interaction and charge transport. The non-nuclear density maxima of IP and superatom states promote strong electronic intermolecular interaction that is unprecedented for the more tightly bound valence states. We expect that the reduced interaction with the atomic cores makes NFE states superior with respect to electron−phonon interaction in transport to the valence states. We predict that by crafting the inner space of hollow molecules through composition of the molecular shell and including dopant atoms in the core, the NFE transport, such as found in semiconductors or metals, will be realized in a new class of molecular materials.

We acknowledge support from the W.M. Keck Foundation, DOE-BES Division of Chemical Sciences, Geosciences, and Biosciences through Grant DE-FG02-09ER16056, and National Science Foundation Grant NSF CHE-0911456. The calculations were performed in the Environmental Molecular Sciences Laboratory at the PNNL, a user facility sponsored by the DOE Office of Biological and Environmental Research.

BIOGRAPHICAL INFORMATION

Min Feng received her Ph.D. degree in 2005 with Prof. H. J. Gao at Institute of Physics, Chinese Academy of Sciences. Subsequently, she came to the University of Pittsburgh (Pitt) as a Postdoctoral Fellow and is currently a Research Assistant Professor. Her research interests include electronic structure and ultrafast dynamics at molecule/surface interfaces.

Jin Zhao received her Ph.D. degree in 2003 with Profs. J. G. Hou and Jinlong Yang at the University of Science and Technology of China (USTC). Subsequently, she joined Hrvoje Petek as a Postdoctoral Fellow and Research Assistant Professor. From 2010, she became a Professor of Physics at USTC, a scientist at International Center for Quantum Design of Functional Materials, Hefei National Laboratory at the Microscale, and an Adjunct Professor at Pitt. The focus of her research is theoretical electronic structure and electron dynamics at surfaces.

Tian Huang received his Ph.D. degree in 2007 with Prof. J. G. Hou from USTC. He is currently a Postdoctoral Fellow at Pitt, where he is studying the electronic structure and dynamics of molecule/solid interfaces.

Xiaoyang Zhu is the Vauquelin Regents Professor of Chemistry at the University of Texas (UT), Austin. He received his Ph.D. from UT-Austin in 1989. Before assuming his current position, he was on the faculty at Southern Illinois University and the University of Minnesota. His research interests include interfacial electron transfer in molecular and nanomaterials.

Hrvoje Petek is a Professor of Physics and Chemistry at Pitt. He received his Ph.D. degree from U.C. Berkeley. Before assuming his current position, he was a Research Associate at the Institute for Molecular Science, and Group Leader at Hitachi Advanced

Research Laboratory. His research interests include ultrafast electronic spectroscopy, microscopy, and dynamics of solid surfaces. He is the Editor-in-Chief of *Progress in Surface Science*.

FOOTNOTES

Address Correspondence to: petek@pitt.edu

REFERENCES

1 Hoffmann, R. A chemical and theoretical way to look at bonding on surfaces. *Rev. Mod. Phys.* **1988**, *60*, 601–628.

2 Silkin, V. M.; Zhao, J.; Guinea, F.; Chulkov, E. V.; Echenique, P. M.; Petek, H. Image potential states in graphene. *Phys. Rev. B* **2009**, *80*, No. 121408.

3 Strocov, V. N.; Blaha, P.; Starnberg, H. I.; Rohlfing, M.; Claessen, R.; Debever, J. M.; Themlin, J. M. Three-dimensional unoccupied band structure of graphite: Very-low-energy electron diffraction and band calculations. *Phys. Rev. B* **2000**, *61*, 4994–5001.

4 Bostwick, A.; McChesney, J.; Ohta, T.; Rotenberg, E.; Seyller, T.; Horn, K. Experimental studies of the electronic structure of graphene. *Prog. Surf. Sci.* **2009**, *84*, 380–413.

5 Geim, A. K. Graphene: Status and prospects. *Science* **2009**, *324*, 1530–1534.

6 Echenique, P. M.; Pendry, J. B. The existence and detection of Rydberg states at surfaces. *J. Phys. C* **1978**, *11*, 2065–2075.

7 Csanyi, G.; Littlewood, P. B.; Nevidomskyy, A. H.; Pickard, C. J.; Simons, B. D. The role of the interlayer state in the electronic structure of superconducting graphite intercalated compounds. *Nat. Phys.* **2005**, *1*, 42–45.

8 Kaskhedikar, N. A.; Maier, J. Lithium storage in carbon nanostructures. *Adv. Mater.* **2009**, *21*, 2664–2680.

9 Chulkov, E. V.; Silkin, V. M.; Echenique, P. M. Image potential states on metal surfaces: Binding energies and wave functions. *Surf. Sci.* **1999**, *437*, 330–352.

10 Fauster, T.; Himpsel, F. J.; Fischer, J. E.; Plummer, E. W. Three-dimensional energy band in graphite and lithium-intercalated graphite. *Phys. Rev. Lett.* **1983**, *51*, 430–433.

11 Lehmann, J.; Merschdorf, M.; Thon, A.; Voll, S.; Pfeiffer, W. Properties and dynamics of the image potential states on graphite investigated by multiphoton photoemission spectroscopy. *Phys. Rev. B* **1999**, *60*, 17037–17045.

12 Bose, S.; Silkin, V. M.; Ohmann, R.; Brihuega, I.; Vitali, L.; Michaelis, C. H.; Mallet, P.; Veuillen, J. Y.; Schneider, M. A.; Chulkov, E. V.; Echenique, P. M.; Kern, K. Image potential states as a quantum probe of graphene interfaces. *New J. Phys.* **2010**, *12*, No. 023028.

13 Posternak, M.; Baldereschi, A.; Freeman, A. J.; Wimmer, E. Prediction of electronic surface states in layered materials: graphite. *Phys. Rev. Lett.* **1984**, *52*, 863–866.

14 Holzwarth, N. A. W.; Louie, S. G.; Rabii, S. X-ray form factors and the electronic structure of graphite. *Phys. Rev. B* **1982**, *26*, 5382–5390.

15 Blase, X.; Rubio, A.; Louie, S. G.; Cohen, M. L. Quasiparticle band structure of bulk hexagonal boron nitride and related systems. *Phys. Rev. B* **1995**, *51*, 6868–6875.

16 Hu, S.; Zhao, J.; Jin, Y.; Yang, J.; Petek, H.; Hou, J. G. Nearly free-electron superatom states of carbon and boron nitride nanotubes. *Nano Lett.* **2010**, *10*, 4830–4838.

17 Meyer, J. C.; Geim, A. K.; Katsnelson, M. I.; Novoselov, K. S.; Booth, T. J.; Roth, S. The structure of suspended graphene sheets. *Nature* **2007**, *446*, 60–63.

18 Feng, M.; Zhao, J.; Petek, H. Atomlike, hollow-core-bound molecular orbitals of C_{60}. *Science* **2008**, *320*, 359–362.

19 Zhu, X. Y.; Dutton, G.; Quinn, D. P.; Lindstrom, C. D.; Schultz, N. E.; Truhlar, D. G. Molecular quantum well at the C_{60}/Au(111) interface. *Phys. Rev. B* **2006**, *74*, No. 241401.

20 Hashizume, T.; Motai, K.; Wang, X. D.; Shinohara, H.; Saito, Y.; Maruyama, Y.; Ohno, K.; Kawazoe, Y.; Nishina, Y.; Pickering, H. W.; Kuk, Y.; Sakurai, T. Intramolecular structures of C_{60} molecules adsorbed on the Cu(111)-(1 × 1) surface. *Phys. Rev. Lett.* **1993**, *71*, 2959–2962.

21 Hou, J. G.; Yang, J.; Wang, H.; Li, Q.; Zeng, C.; Lin, H.; Bing, W.; Chen, D. M.; Zhu, Q. Identifying molecular orientation of individual C_{60} on a Si(111)-(7 × 7) surface. *Phys. Rev. Lett.* **1999**, *83*, 3001–3004.

22 Lu, X.; Grobis, M.; Khoo, K. H.; Louie, S. G.; Crommie, M. F. Spatially mapping the spectral density of a single C_{60} molecule. *Phys. Rev. Lett.* **2003**, *90*, No. 096802.

23 Petek, H.; Ogawa, S. Femtosecond time-resolved two-photon photoemission studies of electron dynamics in metals. *Prog. Surf. Sci.* **1997**, *56*, 239–310.

24 Tautz, F. S. Structure and bonding of large aromatic molecules on noble metal surfaces: The example of PTCDA. *Prog. Surf. Sci.* **2007**, *82*, 479–520.

25 Shipman, S. T.; Garrett-Roe, S.; Szymanski, P.; Yang, A.; Strader, M. L.; Harris, C. B. Determination of band curvatures by angle-resolved two-photon photoemission in thin films of C_{60} on Ag(111). *J. Phys. Chem. B* **2006**, *110*, 10002–10010.

26 Weinelt, M. Time-resolved two-photon photoemission from metal surfaces. *J. Phys.: Condens. Matter* **2002**, *14*, R1099–R1141.

27 Dougherty, D. B.; Maksymovych, P.; Lee, J.; Feng, M.; Petek, H.; Yates, J. T., Jr. Tunneling spectroscopy of Stark-shifted image potential states on Cu and Au surfaces. *Phys. Rev. B* **2007**, *76*, No. 125428.

28 Martins, J. L.; Troullier, N.; Weaver, J. H. Analysis of occupied and empty electronic states of C_{60}. *Chem. Phys. Lett.* **1991**, *180*, 457–460.

29 Yannouleas, C.; Landman, U. Stabilized-jellium description of neutral and multiply charged fullerenes $C^{x\pm}_{60}$. *Chem. Phys. Lett.* **1994**, *217*, 175–185.

30 Pavlyukh, Y.; Berakdar, J. Angular electronic `band structure' of molecules. *Chem. Phys. Lett.* **2009**, *468*, 313–318.

31 Miyamoto, Y.; Saito, S.; Tománek, D. Electronic interwall interactions and charge redistribution in multiwall nanotubes. *Phys. Rev. B* **2001**, *65*, No. 041402.

32 Zhao, J.; Feng, M.; Yang, J.; Petek, H. The superatom states of fullerenes and their hybridization into the nearly free electron bands of fullerites. *ACS Nano* **2009**, *3*, 853–864.

33 Boyle, M.; Hoffmann, K.; Schulz, C. P.; Hertel, I. V.; Levine, R. D.; Campbell, E. E. B. Excitation of Rydberg series in C_{60}. *Phys. Rev. Lett.* **2001**, *87*, No. 273401.

34 Huang, T.; Zhao, J.; Feng, M.; Petek, H.; Yang, S.; Dunsch, L. Superatom orbitals of $Sc_3N@C_{80}$ and their intermolecular hybridization on Cu(110)-(2 × 1)-O surface. *Phys. Rev. B* **2010**, *81*, No. 085434.

35 Feng, M.; Lee, J.; Zhao, J.; Yates, J. T.; Petek, H. Nanoscale templating of close-packed C_{60} nanowires. *J. Am. Chem. Soc.* **2007**, *129*, 12394–12395.

36 Bisio, F.; Nývlt, M.; Franta, J.; Petek, H.; Kirschner, J. Mechanisms of high-order perturbative photoemission from Cu(001). *Phys. Rev. Lett.* **2006**, *96*, No. 087601.

37 Nilius, N.; Wallis, T. M.; Ho, W. Development of one-dimensional band structure in artificial gold chains. *Science* **2002**, *297*, 1853–1856.

38 Crain, J. N.; Pierce, D. T. End states in one-dimensional atom chains. *Science* **2005**, *307*, 703–706.

39 Dutton, G.; Zhu, X.-Y. Unoccupied electronic states in C_{60} thin films probed by two-photon photoemission. *J. Phys. Chem. B* **2002**, *106*, 5975–5981.

40 Dutton, G.; Pu, J.; Truhlar, D. G.; Zhu, X.-Y. Lateral confinement of image electron wavefunction by an interfacial dipole lattice. *J. Chem. Phys.* **2003**, *118*, 4337–4340.

41 Dutton, G.; Quinn, D. P.; Lindstrom, C. D.; Zhu, X. Y. Exciton dynamics at molecule-metal interfaces: C_{60}/Au(111). *Phys. Rev. B* **2005**, *72*, No. 045441.

42 Kera, S.; Yamane, H.; Ueno, N. First-principles measurements of charge mobility in organic semiconductors: Valence hole-vibration coupling in organic ultrathin films. *Prog. Surf. Sci.* **2009**, *84*, 135–154.

43 Horowitz, C. M.; Proetto, C. R.; Pitarke, J. M. Localized versus extended systems in density functional theory: Some lessons from the Kohn-Sham exact exchange potential. *Phys. Rev. B* **2010**, *81*, No. 121106.

44 Lu, N.; Li, Z.; Yang, J. Electronic structure engineering via on-plane chemical functionalization: A comparison study on two-dimensional polysilane and graphane. *J. Phys. Chem. C* **2009**, *113*, 16741–16746.